Technical Sciences, 2024, 27, 409–428

UNIWERSYTET WARMIŃSKO-MAZURSKI W OLSZTYNIE

Yearbook peer-reviewed scientific journal
ISSN 1505-4675
e-ISSN 2083-4527
TECHNICAL SCIENCES
Homepage: https://czasopisma.uwm.edu.pl/index.php/ts/

DOI: https://doi.org/10.31648/ts.10939

ADVANCED, ON-LINE GNSS MULTI-CONSTELLATION MISSION PLANNING AND MULTIPATH MITIGATION TOOL

***Dariusz Tomaszewski*[1], *Jacek Rapiński*[2], *Artur Janowski*[3]**

[1]ORCID: 0000-0001-8170-1156
[2]ORCID: 0000-0002-8954-7963
[3]ORCID: 0000-0002-5535-408X
Department of Geodesy
Faculty of Geoengineering
University of Warmia and Mazury in Olsztyn

Received 20 December 2024, accepted 1 January 2025, available online 2 January 2025.

K e y w o r d s: GNSS Multipath, GNSS precise positioning, Web application, Geospatial analysis.

A b s t r a c t

Despite the growing number of satellites in multi-constellation GNSS positioning systems, the issue of signal availability and quality persists in urban and forest areas. Additionally, obstacles such as high buildings or dense vegetation can lead to severe multipath problems. Various methods have been developed to mitigate the impact of multipath on measurement results, including optimizing antenna placement, antenna type, receiver type, and employing measurement post processing techniques. However, despite these efforts, multipath interference cannot be completely eliminated and can significantly impact positioning accuracy. To tackle this challenge, a tool GNSS MPD for predicting satellite signal obstruction was developed. This tool considers Line of Sight (LOS) vectors between specific locations and satellite positions, as well as obstacle models derived from airborne LiDAR data. The LiDAR data is automatically acquired from geoportal.gov.pl, and an approximate terrain cover model is generated. Satellite obstructions are then validated using a ray casting method. The authors of the study outlined the platform's design and implementation. Subsequently, two experiments were conducted. The first experiment consisted in comparing the obtained satellite visibility scenarios with the results obtained from hemispherical photography. The second study involved performing five daily satellite observations in an area characterized

Correspondence: Dariusz Tomaszewski, Katedra Geodezji, Wydział Geoinżynierii, Uniwersytet Warmińsko-Mazurski, ul. Oczapowskiego 1, 10-719 Olsztyn, e-mail: dariusz.tomaszewski@uwm.edu.pl

by severe terrain obstacles. Based on the receiver's approximate position, satellite visibility scenarios were generated using the developed platform. Static positioning was performed as part of the experiment, producing two sets of results: one using raw receiver observations without modifications, and the other incorporating visibility scenarios from the platform to adjust observation files. The tests were performed in 5 research scenarios. In each of the cases results demonstrated improvements in both accuracy and the success rate of position determination. For success rate, an increase of more than 20% was achieved. In many cases, positioning accuracy improved by more than 50%.

Introduction

Nowadays, we are experiencing a significant increase in the number of GNSS (Global Navigation Satellite Systems) satellites. The available constellations provide visibility of even more than 50 satellites at the same time with an open antenna horizon. On the other hand, with the increasing urbanization, during satellite measurements we experience many terrain obstacles interfering with and distorting GNSS signals. As a result of these unfavorable conditions, observations from satellites deployed in poor geometry and with many reflected signals are processed. This results in a decrease in positioning accuracy or a complete inability to obtain the result. In the following article, the authors dealt with the problem of finding and eliminating signals that were reflected as a result of the multipath phenomenon.

The term "multipath" refers to the impact of reflected signals on the accuracy and reliability of GNSS positioning. The extent of multipath effects varies based on the receiver-antenna setup but can be quantified to a certain degree (GROVES 2013). In pseudorange measurements, NLOS (Non-Line of Sight) signals can introduce errors of up to 20 meters (HOFMANN-WELLENHOF et al. 2012). For carrier phase measurements, the maximum tracking error is about a quarter of the carrier wavelength, translating to maximum errors of 4.8 cm, 6.0 cm, and 6.4 cm for the L1, L2, and L5 carrier phases of GPS satellites, respectively (ROBUSTELLI, PUGLIANO 2019, TEUNISSEN, MONTENBRUCK 2017).

As multipath affects all measured values, its influence affects most of the available positioning models. In the case of absolute positioning, due to large errors in the pseudorange measurement, it causes significant errors in the result (XIE, PETOVELLO 2014). This often happens in urban canyons due to the reflections from structures that do not cause a significant decrease in signal power (KUBO et al. 2020). In the case of differential positioning, multipath is a serious error because it cannot be reduced by measurement differencing. This is due to its nature and close dependence on the measurement location and the proximity of terrain obstacles (PELC-MIECZKOWSKA et al. 2019). It makes multipath uncorrelated in time and space at different antenna locations. For carrier phase differential positioning, multipath introduces several issues. Firstly, it increases the initial search space for resolving ambiguities, leading to longer resolution times. As a result, the accuracy of the vector solution between the reference station and the rover receiver is compromised (SMYRNAIOS et al. 2013, SPILKER et al. 1996). Additionally, multipath may occur not only in the mobile receiver but also at the reference station (RAPIŃSKI et al. 2024, TOMASZEWSKI et al. 2024). Over the years,

a number of solutions have been proposed to minimize and limit the impact of this error on measurement results. They can be divided into 4 groups (TEUNISSEN, MONTENBRUCK 2017):

– antenna type – the first method of multipath mitigation involves the use of a special type of antenna designed to eliminate signals coming from low and negative elevation angles. There are two types of antenna structures. The first is the choke ring antenna, which features a single element surrounded by concentric rings (TRANQUILLA et al. 1994, DANSKIN et al. 2009, KUNYSZ 2003). The second type is the pinwheel antenna. This antenna comprises an array of 12 spiral slots encircled by 11 concentric slot rings (KUNYSZ, 2000a, 2000b). Due to the size of such antennas, they are not practical for rover receivers and are typically used at reference stations;

– receiver type – refers to the signal processing architecture inside the receiver. Work on appropriate signal processing began in the 1990s. During this time, narrow correlator architectures were developed and implemented in Ashtech receivers and later in Leica receivers in an enhanced form (GARIN et al. 1996, GARIN, ROUSSEAU 1997, HATCH et al. 1997). Later on attempts were made for multipath detection using the superresolution concept (WEILL 1998). At the beginning of the 21st century, new concepts related to narrow correlator architecture were presented (IRSIGLER, EISSFELLER 2003), ultimately leading to the development of advanced algorithms such as the Everest Plus implemented by Trimble (PAZIEWSKI 2022);

– antenna placement – the most effective strategy to mitigate multipath interference is to position the antenna in an environment devoid of nearby multipath signal sources or where the likelihood of such occurrences is minimal. This stipulation is essential for the optimal placement of GBAS (Ground Base Augmentation Systems) reference stations (ROTONDO et al. 2015, TEUNISSEN, MONTENBRUCK 2017, PELC-MIECZKOWSKA et al. 2019, KAVAK et al. 1996);

– measurement post-processing – these methods are designed to analyze observational datasets after the measurements have been taken. It is then assumed that the observations may have been contaminated by a multipath and this should be detected and minimized. The first group of such solutions assumes the use of linear combinations: CMC (Code Minus Carrier) or MP (Multipath Pseudorange Observable) (IRSIGLER, EISSFELLER 2003, PAONNI et al. 2008, RAY et al. 2001). The Code-Minus-Carrier (CMC) linear combination is employed based on the premise that multipath interference has a more pronounced impact on code measurements compared to phase measurements. Multipath error values in pseudorange measurements can reach several meters. Conversely, the maximum multipath error for phase measurements will not exceed 6.5 cm. Therefore, a significant difference between the two values indicates a multipath effect. The use of CMC allows for multipath detection in single-frequency receivers. Pseudorange multipath (MP) observable is a linear

combination algorithm designed for dual frequency receivers. It assumes the use of dependencies between signals to determine the influence of multipath on the measurement results. This combination was used in TEQC software to detect and minimize multipath. These combinations are applicable to both kinematic and static receivers. Simpler solutions, particularly in kinematic applications, involve weighting observations based on the principle that the multipath effect is inversely proportional to the satellite's elevation angle or through the analysis of signal-to-noise ratio values (TEUNISSEN, MONTENBRUCK 2017, STRODE, GROVES 2016). The final category can be implemented at reference stations and is known as sidereal filtering. It operates on the premise that multipath effects recur for a given satellite position each sidereal day (IRSIGLER 2010, ROBUSTELLI, PUGLIANO 2018, WANNINGER, MAY 2001). In the case of the reference stations, multipath can be also detected based on post fit carrier phase residuals analysis (PARK et al. 2004, HUNEGNAW et al. 2023).

Over the years, many methods have been presented for minimizing, detecting, or removing from observation sets the measurements contaminated by multipath. However, this complex process still significantly affects GNSS measurement results. The authors of this article have created a web application (GNSS MPD – Global Navigation Satellite Systems Multipath Detector) that allows for the removal of observations that may be affected by multipath. This application predicts NLOS signals from satellites based on the approximate position of the receiver, data from airborne LiDAR, and broadcast satellite positions. The LiDAR data is automatically acquired from geoportal.gov.pl, and then an approximate terrain cover model is generated. Created model represents the terrain obstacles around the receiver antenna. Satellite obstructions are then validated using a raycasting method. As a result of the analyses, a scenario of the probable visibility of satellites is obtained, which can be used to verify the satellites observed during measurements. The article presents the detailed operating principle of the application and the results of two experiments confirming its validity. In the first experiment, satellite visibility scenarios obtained from the GNSS MPD were compared with the results of hemispherical photography. In the second experiment, the results of static positioning were analyzed based on a 5-day observational data set. As part of this experiment, positioning was performed using raw observational data and data filtered using developed scenarios. The analyses were performed for different lengths of observation sessions. Finally, it is shown how reflected signals can affect the positioning results and to what extent one can minimize this impact using the developed application.

Application – GNSS MPD

As a result of the research, the GNSS MPD (Global Navigation Satellite Systems Multipath detector) application was created. The GNSS MPD software predicts NLOS signals from satellites based on the approximate position of the receiver, data from airborne LiDAR, and broadcast satellite positions. The software exists in web form and is currently available on the network of the University of Warmia and Mazury in Olsztyn. An example of its interface screenshot is shown in Figure 1.

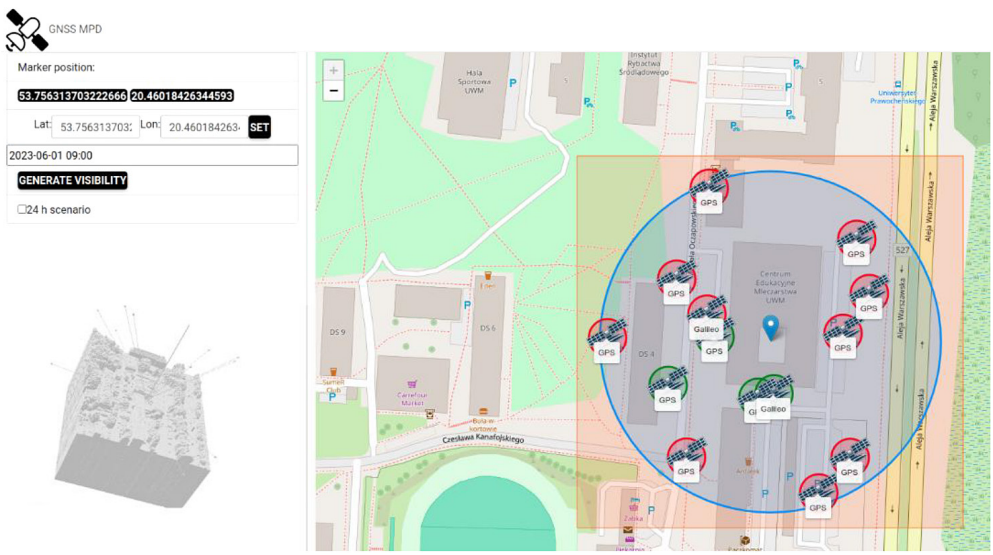

Fig. 1. Interface screenshot of the GNSS MPD application

In the proposed solution, the interface is divided into two parts. On the right side, there is a map where one can mark the position for which the satellite visibility map will be created. This information will be loaded and will appear, as geodetic coordinates, at the top of the screen on the left. To check satellite visibility, the user must set the position with a marker or enter it manually in the form of geodetic coordinates φ and λ. Then, the date and the time of the measurement must be entered in the "date and time" entry on the left. After pressing the "Generate Visibility" button, the antenna's horizon will be marked on the map along with all the satellites located in the space above this horizon. As shown in Figure 1, visible satellites are marked in green and those obscured by terrain obstacles are marked in red. Additionally, for control purposes, a three--dimensional terrain model with marked receiver-satellite vectors appears in the

lower-left corner. To create a satellite visibility scenario, one has to select the "24 h scenario" option. A file will then be created containing information about which satellites should be visible for each measurement epoch over 24 hours from the time specified in the "date and time" entry. The data flow within the GNSS MPD software is depicted by the schema in the Figure 2.

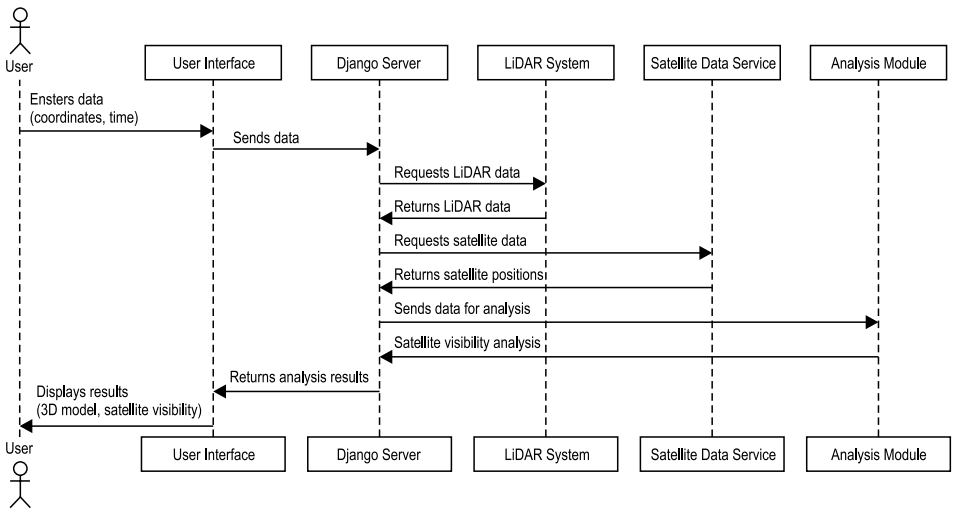

Fig. 2. Schema of the data flow within the GNSS MPD application

Creating an instance of the LiDAR points class requires providing geodetic coordinates (compatible with the WGS84 system, EPSG:4326) of point *P*, which define the center of the study area. It is also necessary to specify the side length of the square defining the area's size and the storage location for the Digital Elevation Model (DEM) description files. The initialization of the LiDAR points object involves the transformation of ellipsoidal coordinates to the Polish local flat coordinate system, PUW 1992 (EPSG:2180), which is the standard for storing LiDAR data (in the Polish Geoportal service) and requirements of the Polish Geoportal for all .laz data queries. Based on this information, the query is sent to the Geoportal, which then returns a list of .laz files necessary to download to ensure complete coverage of the study area. The application checks whether the required files have already been downloaded and stored in its resources. If so, it avoids the downloading process. Otherwise, it downloads the missing files from the Geoportal. Subsequently, the downloaded files are converted 'on the fly' to the .las format, filtered according to the coordinates of the area of interest, and then re-transformed to the WGS84 system, where the application manages defined satellite locations. The location of the planned measurement station

is updated with the elevation of the lowest DEM point within a 1.5-meter radius of the planned location and is further increased by 1.4 m, corresponding to the height of the tripod. Knowing the precise location of the planned measurement station, DEM points in its surroundings, and satellite positions in a unified WGS84 system, it is possible to conduct an analysis of visibility and the limitations caused by DEM points. This analysis is performed using the open3d library, enabling advanced visualization of the geometric scene. An important aspect is the information whether the appropriate point cloud is already on the server. This is a factor that affects the performance of the application. If the appropriate point cloud is on the GNSS MPD server, the model creation and analysis process of the terrain obstacles is carried out in about 3 seconds. In the case when the point cloud has not been downloaded, the process is extended by the data download time. The analysis results are saved in the GLB format (GL Transmission Format Binary), which maintains both: the model's geometry and its textures in a single file. A critical aspect of app-user interaction is the real-time user interface data update via AJAX queries, allowing for dynamic visualization and spatial data analysis. Each user query is handled by creating a temporary file with a unique name, which is provided as a response and, after use, removed from the application's resources, managed by the UUID (Universal Unique Identifier) mechanism. In current form, the point cloud acquisition is based on the use of data from the Polish Geoportal LiDAR data resource. However, the GNSS MPD application was designed in such a way that it is possible to use any point clouds in the appropriate format. It is planned to add a module that allows loading point clouds from conducted measurements.

Experiment

Two experiments were conducted to evaluate the functionality of the designed application. In the first experiment, the satellite visibility maps generated by the application were compared to reference maps obtained from hemispherical photography. In the second experiment, an analysis of the satellite visibility scenarios was performed within the positioning domain. Relative positioning was executed both with and without the visibility scenarios. The tests were conducted in a location with multiple signal obstructions on each side of the receiver antenna. Such an area can be defined as an urban canyon as it can be seen in the Figure 3.

Fig. 3. Location of the measurement point

Sidereal map comparison

As mentioned before, the multipath phenomenon is strongly site-dependent which is why, the knowledge of the exact spatial distribution of terrain obstacles on the antenna horizon is crucial. The hemispherical photography is a powerful tool for modeling such obstacles (PELC-MIECZKOWSKA et al. 2019, 2015). To provide the reference data, the hemispherical photo was taken at the test point with the use of a Canon digital camera with a Sigma Circular Fisheye 4.5 mm F2.8 EX DC lens. The camera has been mounted on a special holder for a geodetic tripod, exactly above the test point and with the nodal point aligned with the antenna horizon. Superimposing the polar plot of satellites above the horizon positions on the hemispherical image allows to determine which satellites should be visible at a given moment and which ones would be obscured by terrain obstacles. Comparison of such an image with the satellite visibility map generated within the GNSS MPD for randomly selected measure epoch is presented in the Figure 4. Satellites that are currently occluded are marked in red, while visible satellites are marked in green on the GNSS MPD visibility map (left image) and in blue on the background of the hemispherical image (right image). In the case of the presented measurement epoch, the compliance of the map generated by GNSS MPD with the reference photo is 100%.

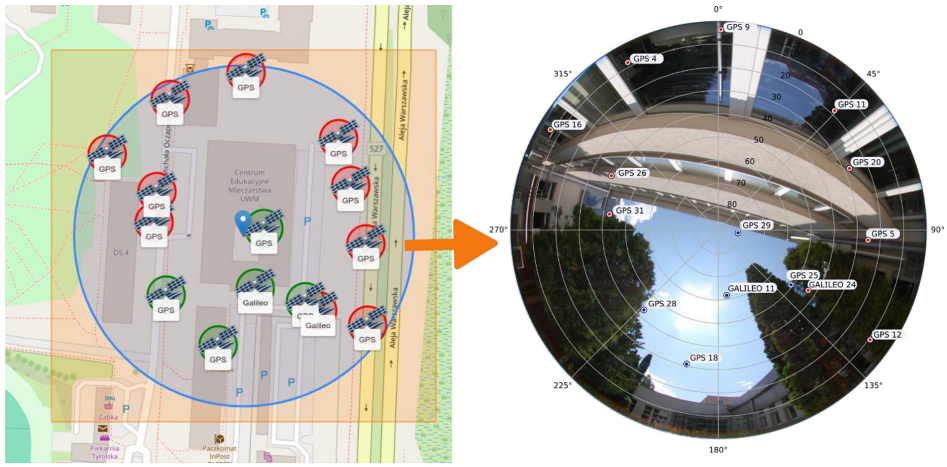

Fig. 4. Satellite visibility map generated within the GNSS MPD and hemispherical photography

In the next step, daily sideral maps were generated using both: GNSS MPD application and an algorithm based on hemispherical photography. Those maps for June 1, 2023, are visible in the Figure 5.

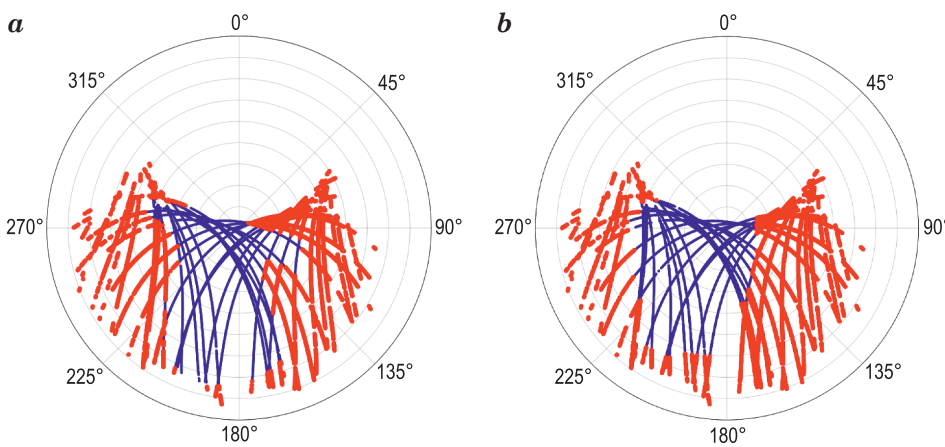

Fig. 5. Daily sideral maps generated using: GNSS MPD application (*a*) and hemispherical photography (*b*)

Based on these maps, one can see that the algorithms are highly consistent. Significant differences can only be noticed in the area where the obstacles are caused by tall bushes (around an azimuth of 140° and an elevation of 65° and around an azimuth of 240° and an elevation of 50°). Then a statistical analysis of the developed sky maps was performed (Fig. 6). Out of all 86,400 measurement

epochs (one day with an interval of 1 s), for almost 80,000 epochs both models are consistent. Errors were detected in 6,400 observations, which gives only 7.4% of epochs. In these epochs, the average error was 20%, which, with an average number of satellites above the horizon of 15, gives 3 satellites in each epoch.

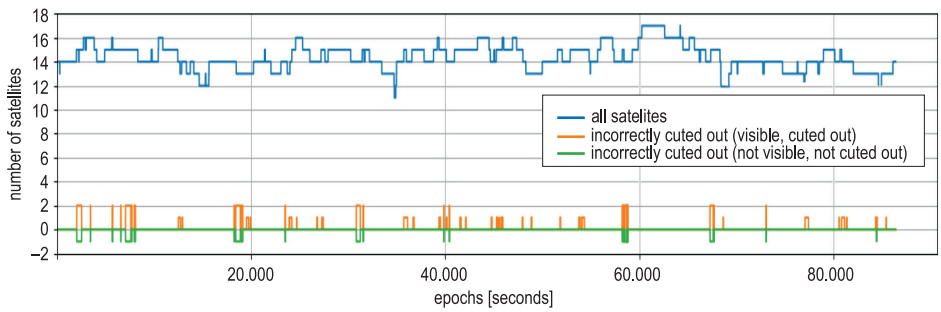

Fig. 6. Statistical analysis of the developed sky maps

Considering the diverse nature of the curtains and the extremely challenging measurement conditions, the results obtained can be regarded as very good. Further analysis tested the proposed method in the position domain.

Positioning experiment

The Javad Alpha receiver with an Ashtech 111661 antenna was used for the study. For the purposes of the study, the receiver had a multipath filter turned on. Observations were made using the GPS, Galileo, and Glonass systems. Five 24-hour observation sessions were conducted from June 1 to June 5, 2023, with a one-second interval. For these days, satellite visibility scenarios were prepared based on the approximate coordinates of the antenna. These scenarios were used to remove from the observation files measurements from satellites that should not be visible due to field obstructions. In this way, two sets of measurement data were obtained. The first set contained raw observations directly from the measurements, and the second set contained observations with the obstructed satellite measurements removed. The stored files were then divided into sets with different session lengths:

– 15 minutes,
– 30 minutes,
– 1 hour,
– 2 hours,
– 4 hours.

Both variants for all session lengths were aligned based on two neighboring ASG EUPOS network stations (LAMA, OPNT) and one virtual reference station (VRS1). For both variants and all session lengths, coordinates were calculated in post processing based on two neighboring stations of the ASG-EUPOS network (LAMA, OPNT) and one virtual reference station (V100) – Figure 7. Individual vectors lengths are presented in the Table 1. For the purposes of the study, the designated point was called P06.

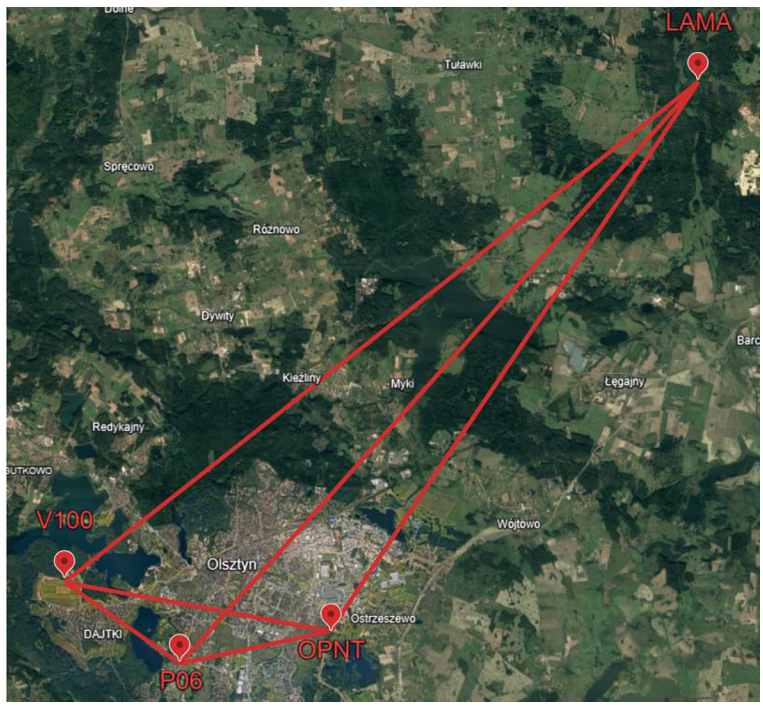

Fig. 7. Sketch of the test network with the location of the measurement point

Table 1

GNSS vectors of the adjusted network

Vector	Length [m]
V100 – LAMA	21,282,966
P06 – LAMA	20,493,552
OPNT – LAMA	17,468,093
OPNT – V100	6,892,789
P06 – V100	3,592,596
P06 – OPNT	3,909,363

The reference coordinates were verified using two methods. First, the coordinates of the P06 point were determined through post-processing of data from five 24-hour static sessions. The results of these sessions showed no more than a 0.02 m difference for each component of the WGS84 *X*, *Y*, *Z* coordinates. Additionally, the results obtained using classical methods were validated by measuring a polygon trace established on both sides. The obtained coordinates were then transformed into the ENU (East-North-Up) rectangular coordinate system. These coordinates served as a reference value for the conducted research. The calculation results for 15-minute sessions are shown in the Figure 8.

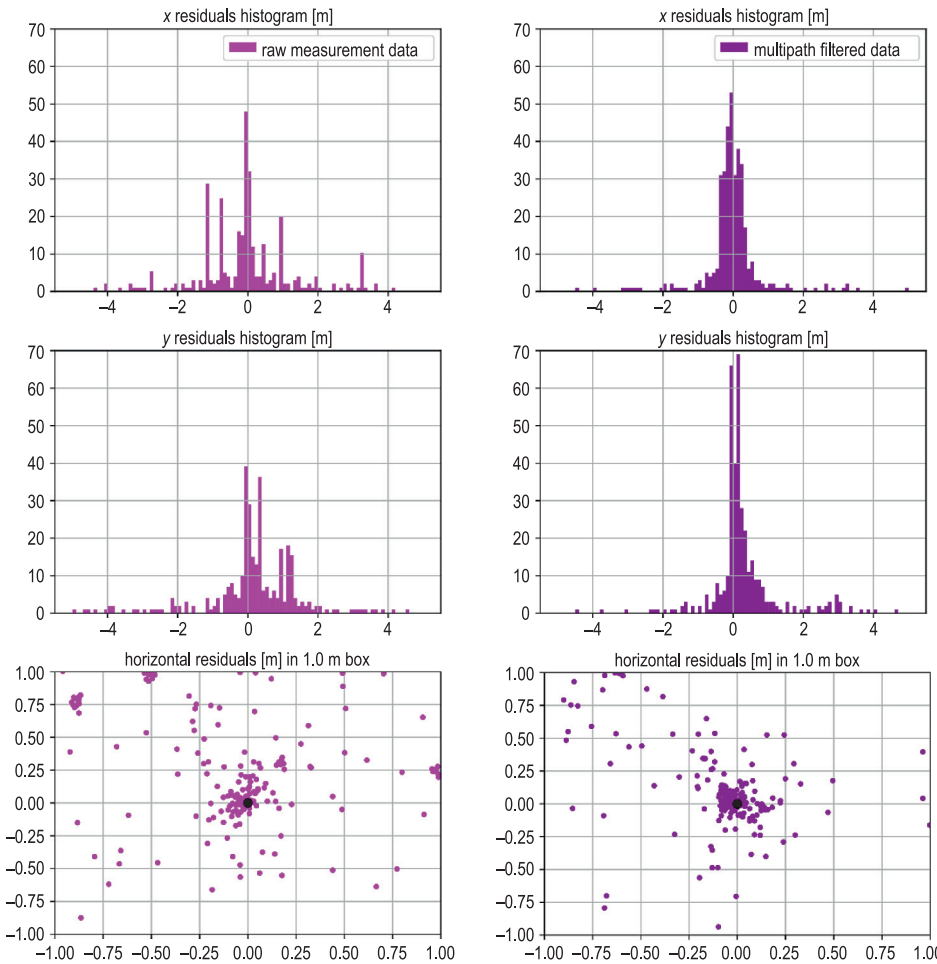

Fig. 8. Residuals of *X* and *Y* coordinates for 15-minute static sessions conducted of raw and multipath filtered data (description in text)

During the analysis of the results from 15-minute sessions, an attempt was made to determine coordinates in 480 sessions. For the raw data set, 325 measurement sessions were calculated. In the case of the filtered data, success was achieved in 369 sessions. These values represent 67.7% and 76.8% of the total set, respectively. Figure 8 shows the residuals x and y of the plane rectangular coordinates. The results from processing the raw observations are marked in pink on the right side. The results for the data set filtered using the designed application are shown in purple on the left side. In the results of raw observational data, one can notice a set of clustered incorrectly resolved sessions with x residuals at the level of -1.2 m, -0.8 m, 1.0 m and even 3.2 m and with y residuals at the level of 1.0-1.3 m. This may suggest that there were periods during which a reflected satellite signal was observed which disturbed the correct solution. Such situations did not occur in the filtered results. In this case, the random sets clustered around zero. both sets had results that deviated significantly from the correct position with residuals above 2.0 m. In the case of raw data, the average residual values for the x and y coordinates were 0.779 m and 0.982 m, respectively. While for the filtered data they were 0.438 m and 0.414 m.

In the raw data for 30-minute observations, 149 out of 240 measurement sessions were resolved, representing 62.8 percent of all sessions. In the case of filtered data, 204 sessions were resolved, which constitutes 85% of the set. Figure 9 shows the residuals x and y of the plane rectangular coordinates. In the case of filtered data, a similar phenomenon can be observed as with the results from 15-minute sessions. Sets of clustered incorrectly resolved sessions with x residuals at the level of -1.0 m, -0.5 m, 1.0 m and with y residuals at the level of 0.5 m, 0.9 – 1.2 m can be noticed. Similarly, it suggests that for such session lengths the reflected signals caused a shift in the positioning results. One can notice a significant reduction in the number of sessions in which position errors were over 2.0 m. In the case of raw data, the average residual values for the x and y coordinates were 0.525 m and 0.551 m, respectively. While for the filtered data they were 0.358 m and 0.327 m.

In the case of 1 hour data sets, in both examined cases, 102 results were obtained from 120 available observation sessions (85%). Figure 10 shows the residuals x and y of the plane rectangular coordinates. In the results from raw observations, it can be noticed that there are observations clustering around significant residuals. However, this phenomenon causes smaller positioning errors, that in the case of shorter sessions, as their absolute value does not exceed 1.1 m. It should be noted that an error of this magnitude in an hour-long static session represents a very high positioning error. In the case of filtered sessions, only in 3 cases the absolute value of positioning residuals exceeded 0.5 m. These results are reflected in the average values of positioning residuals. In the case

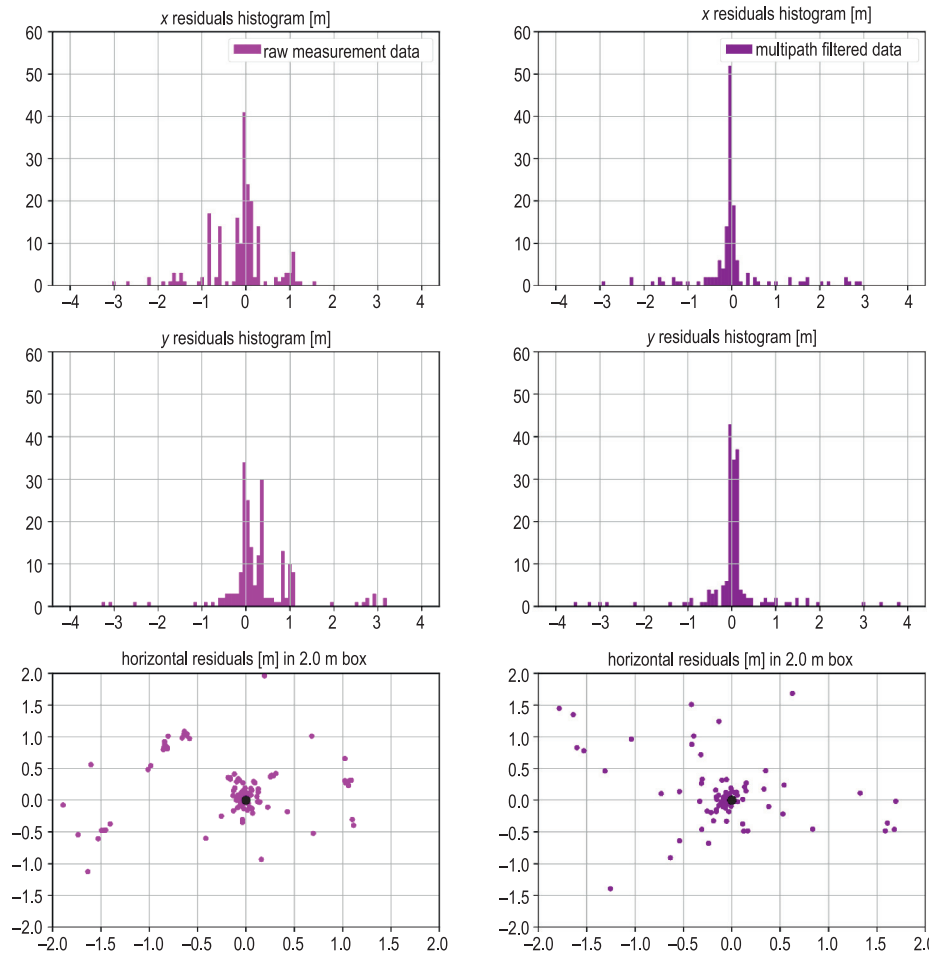

Fig. 9. Residuals of X and Y coordinates for 30-minute static sessions conducted of raw and multipath filtered data (description in text)

of raw data sessions for the x and y coordinates, these values were 0.339 m and 0.391 m, respectively. While for the results from the filtered data, the average positioning residuals were 0.147 m and 0.120 m, respectively.

In the case of 2-hour observations, almost all sessions were post-processed successfully in both cases. Solutions from 57 sessions and 59 sessions out of 60 were obtained for the raw and filtered data, respectively. Figure 11 shows the residuals x and y of the plane rectangular coordinates. The presumed influence of reflected signals can again be seen in the results from the raw observational data. One can still see results that deviate significantly from the reference value. In 13 sessions, there are position residuals ranging in absolute

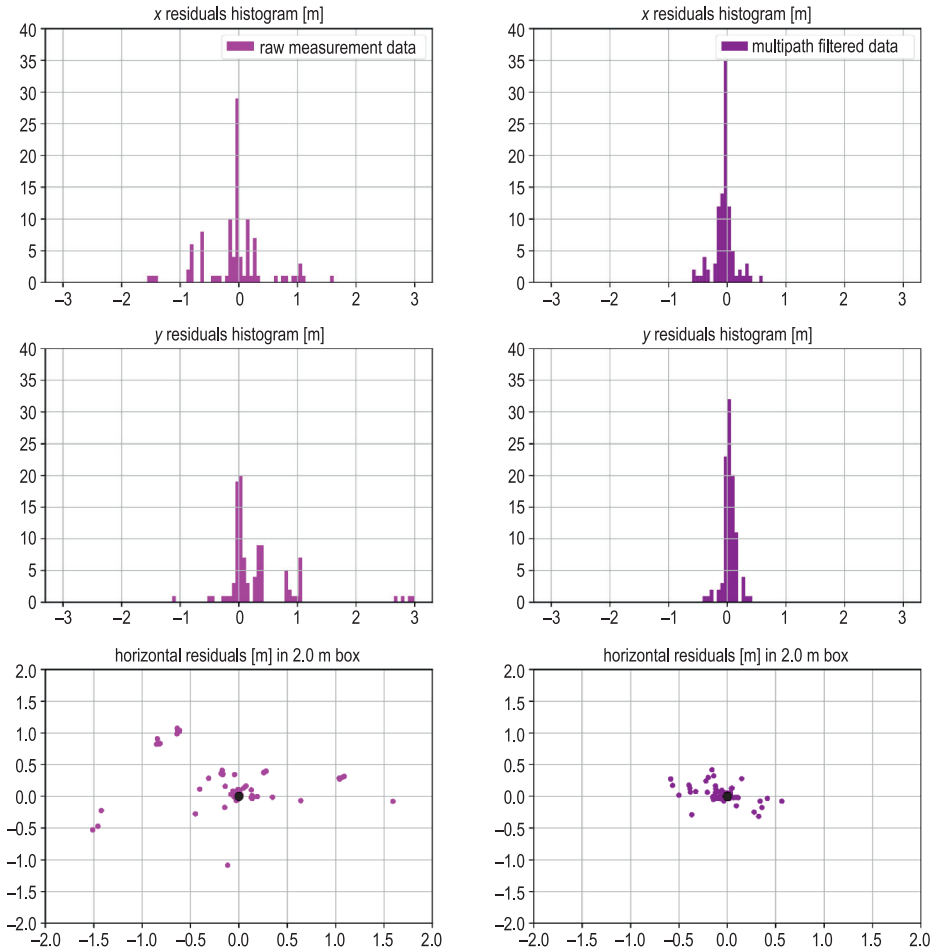

Fig. 10. Residuals of *X* and *Y* coordinates for 1 hour static sessions conducted of raw and multipath filtered data (description in text)

value from 0.5 m to 1.0 m. This constitutes nearly 23% of all results obtained from a single tested set. This situation does not occur in the case of filtered data, where only in 5 sessions the residuals exceeded 0.25 m. In the case of raw data, the average residual values for the *x* and *y* coordinates were 0.289 m and 0.383 m, respectively. While for the filtered data they were 0.099 m and 0.092 m.

In the case of 4-hour sessions, all 30 measurement sessions were adjusted for both examined cases. Figure 12 shows the residuals in the *x* and *y* plane rectangular coordinates. Analyzing the obtained results, it can be noticed that in the case of calculations performed on raw data, there are still sessions with high position residuals. Despite 4-hour measurements, 9 sessions still had

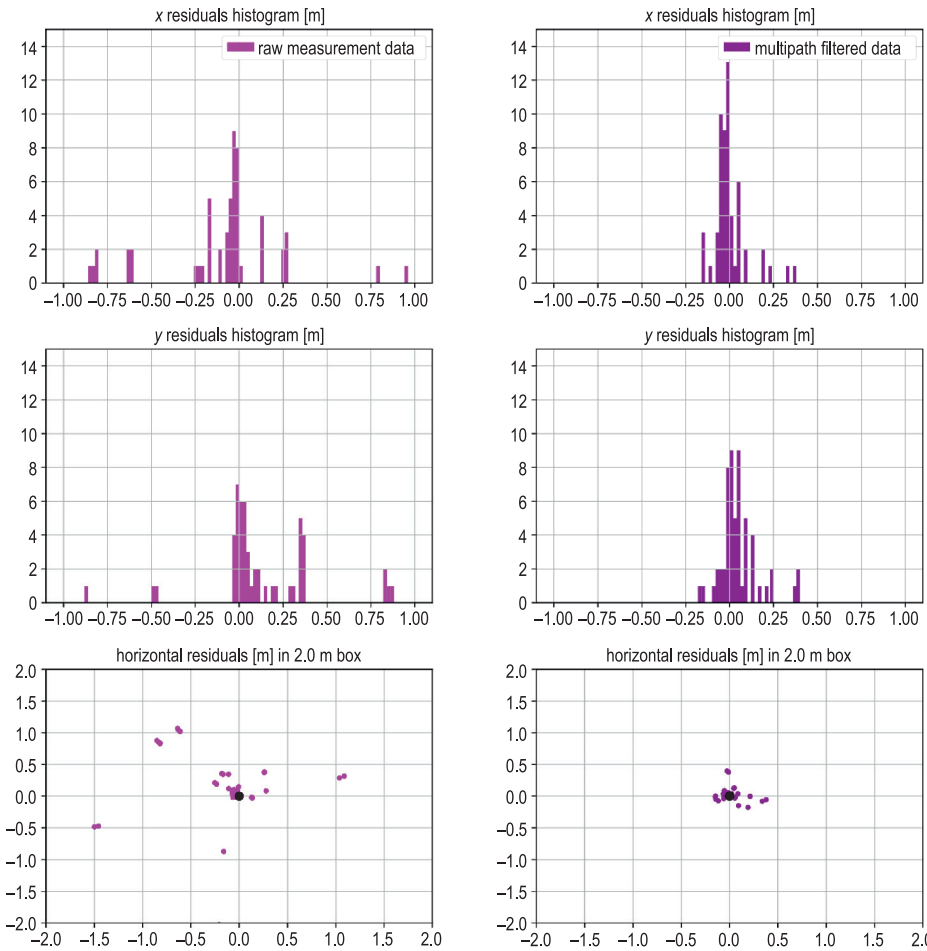

Fig. 11. Residuals of X and Y coordinates for 2 hour static sessions conducted of raw and multipath filtered data (description in text)

errors above 0.5 m. In the case of filtered data, the results do not exhibit such large errors. One can notice 4 sessions for which the residuals are greater than 0.25 m. For raw data, the average residual values for the x and y coordinates were 0.267 m and 0.308 m, respectively, while for the filtered data, they were 0.047 m and 0.046 m. The summary of the results from all performed tests is given in Table 2.

As it can be noticed, the use of filtering proposed by the application improved both the accuracy in all proposed measurement scenarios. In tests conducted on 15-minute data, the average accuracy increased by 50.8%. While in 4-hour sessions the same value was 83.7%. This is a significant increase in accuracy that may indicate the validity of used method.

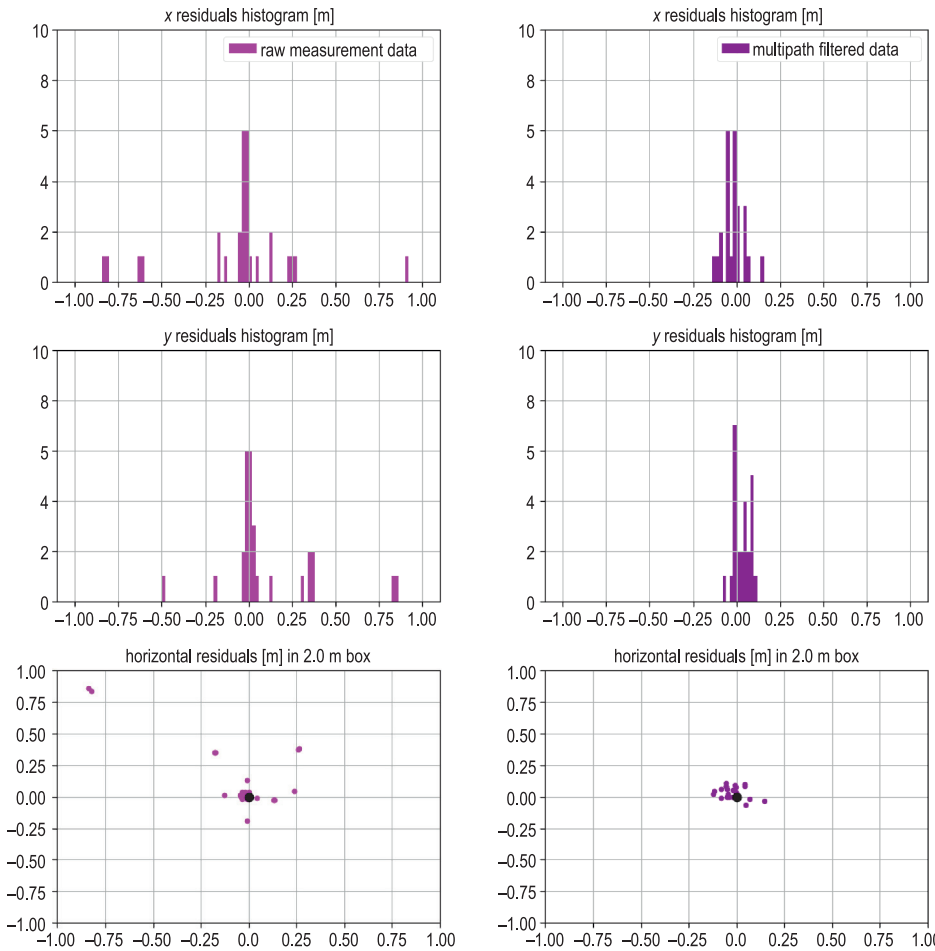

Fig. 12. Residuals of X and Y coordinates for 4 hour static sessions conducted of raw and multipath filtered data (description in text)

Table 2

Summary of the results from all performed tests

Session time	Raw data			GNSS MPD filtered data		
	X average residual [m]	Y average residual [m]	success rate [%]	X average residual [m]	Y average residual [m]	success rate [%]
15 minutes	0.779	0.982	67.7	0.438	0.414	76.8
30 minutes	0.525	0.551	62.8	0.358	0.321	85.0
1 hour	0.339	0.391	85.0	0.147	0.120	85.0
2 hour	0.289	0.383	95.0	0.099	0.092	98.0
4 hour	0.267	0.308	100.0	0.047	0.046	100.0

Discussion

The study investigates the development and evaluation of a GNSS MPD software, designed to predict and mitigate multipath interference in GNSS positioning. This tool integrates airborne LiDAR data and satellite positions to generate a terrain obstacles model, aiding in the prediction of satellite signal obstructions. Two primary experiments were conducted to validate its effectiveness: comparing visibility scenarios with hemispherical photography and conducting static positioning experiments in challenging environments.

A comparative analysis of scenarios generated from hemispherical photography and MPD GNSS software revealed satisfactory agreement between both models. Detected difference in obstructed signal was 7.4%. This value may be attributed to differences in acquisition times between the two data sets or the fact that the MPD model relies on approximate coordinates, while the hemispherical photography model is based on a hemispherical photo taken directly at the measurement point. In measurement epochs where differences were detected, the variance amounted to approximately three satellites, with a maximum of two satellites incorrectly included and one incorrectly excluded. The second study aimed to determine the actual impact of using satellite visibility scenarios on positioning results. In this experiment, static sessions were conducted under conditions with limited satellite visibility in five session duration variants (15 minutes, 30 minutes, 1 hour, 2 hours, and 4 hours). In 15-minute sessions, an increase in the success rate of position determination by 9.1% was observed, along with an approximate 50% increase in horizontal accuracy. In 30-minute sessions, the success rate of position determination increased by 22.2%, with an approximate 36% improvement in horizontal accuracy. In measurement sessions lasting one hour or longer, the increase in the success rate of calculated positioning results was not significant, but there was still a noticeable improvement in positioning accuracy. For 1-hour, 2-hour, and 4-hour sessions, the average accuracy increased by 63%, 71%, and 84%, respectively. Based on both studies, it can be concluded that satellite visibility models created in the GNSS MPD software correspond well to proven methods for creating satellite visibility scenarios. Furthermore, using the obtained scenarios in challenging field conditions enhances both the accuracy and success rate of positioning. Future work will involve using the proposed solution in precise one-epoch kinematic positioning of moving objects. This research will evaluate the performance of GNSS MPD in variable field conditions and help optimize the computational algorithm.

Conclusions

Based on the conducted research, it is evident that the satellite visibility models generated by the GNSS MPD software align well with established methods for creating satellite visibility scenarios. The application of these scenarios in difficult/challenging field conditions has been shown to enhance both: the accuracy and the success rate of positioning. Future authors research will focus on employing this proposed solution for precise single-epoch kinematic positioning of moving objects. This endeavor will assess the performance of the GNSS MPD in diverse field conditions and contribute to optimizing the computational algorithm.

References

DANSKIN S., BETTINGER P., JORDAN T. 2009. *Multipath mitigation under forest canopies: A choke ring antenna solution*. Forest Science, 55(2): 109-116.

GARIN L., ROUSSEAU J.-M. 1997. *Enhanced strobe correlator multipath rejection for code & carrier*. Proceedings of the 10th International Technical Meeting of the Satellite Division of The Institute of Navigation (ION GPS 1997), p. 559-568.

GARIN L., VAN DIGGELEN F., ROUSSEAU J.-M. 1996. *Strobe & edge correlator multipath mitigation for code*. Proceedings of the 9th International Technical Meeting of the Satellite Division of the Institute of Navigation (ION GPS 1996), p. 657-664.

GROVES P.D. 2013. *Future trends in integrated navigation*. Inside GNSs, 8(2): 44-49.

HATCH R.R., KEEGAN R.G., STANSELL T.A. 1997. *Leica's code and phase multipath mitigation techniques*. Proceedings of the 1997 National Technical Meeting of The Institute of Navigation, p. 217-225.

HOFMANN-WELLENHOF B., LICHTENEGGER H., COLLINS J. 2012. *Global positioning system: theory and practic*e. Springer Science & Business Media.

HUNEGNAW A., DUMAN H., EJIGU Y.G., BALTACI H., DOUŠA J., TEFERLE F.N. 2023. *On the impact of GPS multipath correction maps and post-fit residuals on slant wet delays for tracking severe weather events*. Atmosphere, 14(2): 219.

IRSIGLER M. 2010. *Characterization of multipath phase rates in different multipath environments*. GPS Solutions, 14(4): 305-317.

IRSIGLER M., EISSFELLER B. 2003. *Comparison of multipath mitigation techniques with consideration of future signal structure*s. Proceedings of the 16th International Technical Meeting of the Satellite Division of The Institute of Navigation (ION GPS/GNSS 2003), p. 2584-2592.

KAVAK A., XU G., VOGEL W.J. 1996. *GPS multipath fade measurements to determine l-band ground reflectivity properties*. Proceedings of the 20th NASA Propagation Experimenters Meeting.

KUBO N., KOBAYASHI K., FURUKAWA R. 2020. *GNSS multipath detection using continuous time-series c/n0*. Sensors, 20(14): 4059.

KUNYSZ W. 2000a. *High performance GPS pinwheel antenna*. Proceedings of the 13th International Technical Meeting of the Satellite Division of The Institute of Navigation (ION GPS 2000), p. 2506-2511.

KUNYSZ W. 2000b. *A novel GPS survey antenna*. Proceedings of the 2000 National Technical Meeting of The Institute of Navigation, p. 698-705.

KUNYSZ W. 2003. *A three dimensional choke ring ground plane antenna*. Proceedings of the 16th International Technical Meeting of The Satellite Division of The Institute of Navigation (ION GPS/GNSS 2003), p. 1883-1888.

PAONNI M., AVILA-RODRIGUEZ J.-A., PANY T., HEIN G.W., EISSFELLER B. 2008. *Looking for an optimum S-curve shaping of the different MBOC implementations*. Navigation, 55(4): 255-266.

PARK K.-D., NEREM R., SCHENEWERK M., DAVIS J. 2004. *Site-specific multipath characteristics of global IGS and CORS GPS sites*. Journal of Geodesy, 77: 799-803.

PAZIEWSKI J. 2022. *Multi-constellation single-frequency ionospheric-free precise point positioning with low-cost receivers*. GPS Solutions, 26(1): 23.

PELC-MIECZKOWSKA R., JANICKA J., BEDNARCZYK M., TOMASZEWSKI D. 2015. *Comparison of selected data acquisition methods for GNSS terrain obstacles modeling*. Acta Geodynamica et Geomaterialia, 12(3): 307- 315.

PELC-MIECZKOWSKA R., TOMASZEWSKI D., BEDNARCZYK M. 2019. *GNSS obstacle mapping as a data preprocessing tool for positioning in a multipath environment*. Measurement Science and Technology, 31(1): 015017.

RAPIŃSKI J., TOMASZEWSKI D., PELC-MIECZKOWSKA R. 2024. *Analysis of multipath changes in the polish permanent GNSS stations network*. Remote Sensing, 16(9): 1617.

RAY J., CANNON M., FENTON P. 2001. *GPS code and carrier multipath mitigation using a multiantenna system*. IEEE Transactions on Aerospace and Electronic Systems, 37(1): 183-195.

ROBUSTELLI U., PUGLIANO G. 2018. *GNSS code multipath short-time fourier transform analysis. Navigatio*n: Journal of The Institute of Navigation, 65(3): 353-362.

ROBUSTELLI U., PUGLIANO G. 2019. *Code multipath analysis of Galileo FOC satellites by time-frequency representation*. Applied Geomatics, 11(1): 69-80.

ROTONDO G., THEVENON P., MILNER C., MACABIAU C., FELUX M., HORNBOSTEL A., CIRCIU M.-S. 2015. *Methodology for determining Pseudorange noise and multipath models for a multi-constellation, multi-frequency GBAS system*. Proceedings of the 2015 International Technical Meeting of The Institute of Navigation, p. 383-392.

SMYRNAIOS M., SCHN S., LISO M., JIN S. 2013. *Multipath propagation, characterization and modeling in GNSS*. Geodetic Sciences Observations, Modeling and Applications, p. 99-125. https://doi.org/10.5772/54567

SPILKER JR J.J., AXELRAD P., PARKINSON B.W., ENGE P. 1996. *Global positioning system: theory and applications*. Vol. I. American Institute of Aeronautics and Astronautics. https://doi.org/10.2514/4.866388

STRODE P.R., GROVES P.D. 2016. *GNSS multipath detection using three-frequency signal-to-noise measurements*. GPS Solutions, 20(3): 399-412.

TEUNISSEN P.J., MONTENBRUCK O. 2017. *Springer handbook of global navigation satellite systems*. Vol. 10. Springer, Cham. https://doi.org/10.1007/978-3-319-42928-1

TOMASZEWSKI D., PELC-MIECZKOWSKA R., RAPIŃSKI J. 2024. *On the GPS signal multipath at ASG-EUPOS stations*. Journal of Applied Geodesy, 18(3): 553-571. https://doi.org/10.1515/jag-2023-0090

TRANQUILLA J.M., CARR J., AL-RIZZO H.M. 1994. *Analysis of a choke ring groundplane for multipath control in global positioning system (GPS) application*s. IEEE Transactions on antennas and propagation, 42(7): 905-911.

WANNINGER L., MAY M. 2001. *Carrier-phase multipath calibration of GPS reference stations*. Navigation, 48(2): 112-124.

WEILL L. R. 1998. *Application of superresolution concepts to the GPS multipath mitigation problem*. Proceedings of the 1998 National Technical Meeting of The Institute of Navigation, p. 673-682.

XIE P., PETOVELLO M.G. 2014. *Measuring GNSS multipath distributions in urban canyon environments*. IEEE Transactions on Instrumentation and Measurement, 64(2): 366-377.